Simulation of Plasma Injector Module for Plasma Assisted Combustion in scramjet

Ancelin Rocamora, Julien Labaune, Aymeric Bourlet, Christophe O Laux, Fabien Tholin

▶ **To cite this version:**

Ancelin Rocamora, Julien Labaune, Aymeric Bourlet, Christophe O Laux, Fabien Tholin. Simulation of Plasma Injector Module for Plasma Assisted Combustion in scramjet. EUCASS-CEAS 2023 10th European Conference for Aerospace Sciences (EUCASS) - 9th conference of the Council of European Aerospace Societies (CEAS)., EUCASS AISBL, Jul 2023, Lausanne, Switzerland. 10.13009/EUCASS2023-419 . hal-04230042

HAL Id: hal-04230042
https://hal.science/hal-04230042v1

Submitted on 5 Oct 2023

HAL is a multi-disciplinary open access archive for the deposit and dissemination of scientific research documents, whether they are published or not. The documents may come from teaching and research institutions in France or abroad, or from public or private research centers.

L'archive ouverte pluridisciplinaire **HAL**, est destinée au dépôt et à la diffusion de documents scientifiques de niveau recherche, publiés ou non, émanant des établissements d'enseignement et de recherche français ou étrangers, des laboratoires publics ou privés.

Distributed under a Creative Commons Attribution 4.0 International License

DOI: 10.13009/EUCASS2023-419
Aerospace Europe Conference 2023 – 10TH EUCASS – 9TH CEAS

Simulation of Plasma Injector Module for Plasma Assisted Combustion in scramjet

Ancelin Rocamora[⋆†] *and Julien Labaune*[⋆] *and Aymeric Bourlet*[⋆] *and Christophe Laux*[⋆⋆] *and Fabien Tholin*[⋆]
[⋆]*ONERA*
Université Paris Saclay F-91123 Palaiseau - France
[⋆⋆]*Laboratoire EM2C*
CNRS-CentraleSupélec, Université Paris-Saclay, Gif-sur-Yvette - France
First Author Email · ancelin.rocamora@onera.fr
[†]Corresponding author

Abstract

Plasma-assisted combustion (PAC) is an exciting way of improving the stabilisation of supersonic combustion and fuel-oxidant mixing in a scramjet, especially during transient modes. However, coupling hydrodynamic and electric physic makes the numerical approach difficult. The article aims to model the operation of a Plasma Injector Module (PIM) developed on the SBR-50 test facility by S. Leonov in a complete combustion chamber within a reasonable computing time. The approach will reproduce similar arc morphology as the experiment. Then the mixing effect efficiency will be studied through the arc positioning. Finally, the mechanism of one restrike will be detailed.

1. Introduction

Scramjets are airbreathing jet engines with no moving parts allowing hypersonic flight (Mach > 5) by handling a combustion in a supersonic flow. One of the promising possibilities to improve and stabilize the combustion is the PAC fieldwith DC (Direct Current) arc discharge as studied by A. Firsov [1], and S. Leonov [2]. The arc is helpful during the scramjet's most unfavourable phase of flight: its acceleration towards hypersonic flight [3]. However, until now, this method has essentially been studied through test facility experiments. These test campaigns are prosperous and have made it possible to test numerous geometries of combustion chambers and plasma actuators. Still, the means of the investigation remain limited by the phenomena's dimensions and time scales, and the complex multiphysics coupling between the electric arc and the reactive flows still requires investigations to design such PAC actuators properly. Indeed, phenomena with a characteristic time of 10^{-5} s and space scale of 10^{-1} m have to be simulate with a 10^{-9} s time step and mcell size of 10^{-4} m. In this work, the supersonic facility SBR-50 of Notre Dame University equipped with an original system known as PIM is simulated with some physical condition adaptation [4]. Such a system, described in Section 3, is composed of an anode surrounding the fuel injector itself insulated from the grounded wall by a ceramic. A great advantage provided by this technology is to place the plasma in the mixing layer and potentially improve the mixing between fuel and oxidant.

A magneto-hydrodynamic (MHD) code described in Section 2 is used to solve the physics of this plasma actuator. The quasi-neutral approximation (no space charge in the domain) makes it possible to model the electric arc with time steps and spatial discretisation compatible with reactive CFD (Computational Fluid Dynamic) calculations on large 3D geometries such as the combustion chamber of a scramjet.

The first goal of the article is to reproduce numerically the morphology of the arc observed in [5] and to study in detail the complex coupling between the plasma and the turbulent flow. The second goal is to evaluate the expected mixing effect of the arc discharge on fuel and oxidant that was observed [6].

2. Physics and equations

Two numerical codes have been used for this study. One to solve the Navier-Stokes equations and the other one to solve the current conservation equation. These two codes are coupled in parallel with a coupling software that enables exchanges of fields and source terms.

Copyright © 2023 by ONERA. Posted on line by the EUCASS association with permission.

DOI: 10.13009/EUCASS2023-419

2.1 Fluid equations

To solve the gas flow in the supersonic combustor, the multi-species Navier-Stokes equations are solved in compressible and reactive states as described by G. Pelletier [7] while adding the production term ω_α for the species α, and the Joule heating term ω_{Joule} to take into account the plasma effects on the flow. Their resolution is performed by the reacting gas solver CHARME, implemented in the CEDRE (Calcul d'Écoulements Diphasiques Réactifs pour l'Énergétique) semi-industrial multiphysics code [8], developed by the Office national d'études et de recherches aérospatiales (ONERA).

$$\frac{\partial}{\partial t}\left(\overline{\rho}\tilde{Y}_\alpha\right) + \frac{\partial}{\partial x_j}\left(\overline{\rho}\tilde{u}_j\tilde{Y}_\alpha\right) = \frac{\partial}{\partial x_j}\left(-\overline{\rho u_j'' Y_\alpha''} - \overline{J}_j^\alpha\right) + \overline{\dot{\omega}}_\alpha \tag{1}$$

$$\frac{\partial}{\partial t}\left(\overline{\rho}\tilde{u}_i\right) + \frac{\partial}{\partial x_j}\left(\overline{\rho}\tilde{u}_j\tilde{u}_i\right) = \frac{\partial}{\partial x_j}\left(-\overline{\rho u_j'' u_i''} - \overline{P}\delta_{ij} + \overline{\tau}_{ij}\right) \tag{2}$$

$$\frac{\partial}{\partial t}\left(\overline{\rho}\tilde{e}_t\right) + \frac{\partial}{\partial x_j}\left(\overline{\rho}\tilde{u}_j\tilde{e}_t\right) = \frac{\partial}{\partial x_j}\left(-\overline{\rho u_j'' e_t''} - \overline{J}_j^{e_t} + \tilde{\sigma}_{ij}\tilde{u}_i\right) + \omega_{Joule} \tag{3}$$

In mass balance equation (1) ρ [kg·m^{-3}] is the density; Y_α [-] is the mass fraction of species α; u_j [kg·m·s^{-1}] is the j-component of the fluid velocity vector u; J_j^α [kg·m^{-2}·s^{-1}] is the j-component of the molecular diffusion flux for the chemical species α; ω_α [kg·m^{-3}s^{-1}] is the production rate of species α if positive or the consumption rate if negative. In the momentum balance equation (2), P [Pa] denotes the pressure tensor, and τ_{ij} [Pa] is the viscous stress tensor term. In energy conservation equation (3), e_t [J·kg^{-1}] is the total energy per unit of mass and $J_j^{e_t}$ [J·s^{-1}·m^{-2}] is the j-component of the total energy molecular flux. The term ω_{Joule} [J·m^{-3}·s^{-1}] denotes the volumetric heating in the fluid by the Joule effect.

Any letter topped by a bar means that the associated quantity is Reynolds averaged, while any letter topped by a tilde means that it is a Favre mass-weighted averaged quantity. The latter is constructed by dividing the Reynolds average of the product of the density and this quantity by the Reynolds average of the density. The associated flux of a quantity is constructed by subtracting its Favre average value from the quantity.

For this study, to reduce complexitiy, non-reactive states are use. In addition, LTE (Local Thermodynamic Equilibrium) is assumed therefore it is possible to use a single species that represents the air. The thermodynamic properties of air at LTE have been tabulated as a function of temperature and pressure based on the work of A. D'Angola [9]. The temperature and pressure ranges are respectively 100 – 20 000 K and 10^2 – 10^8 Pa, which is more than enough in our case. The turbulence model used is the LES (Large Eddy Simulation) model with a sub-mesh Smagorinsky model using constants put in Table 1.

Table 1: Sub grid model constant for LES

	Values
Prandtl constant c_μ	0.09
Karman constant κ	0.41
Turbulent Prandtl number Pr_l	0.9
Turbulent Schidt number $S\,c_l$	0.9

2.2 Electric equation

For the computation of the Joule heating term in 3, the current conservation equation (4) should be solved. That is done by TARANIS, a node-centred plasma solver code developed at ONERA to model lightning and plasma discharges. The quasi-neutrality of the electric arc is assumed. In our simulation, the magnetic field has been neglected due to the low current level of 10 A.

$$\boldsymbol{\nabla} \cdot \mathbf{J_q} = 0 \tag{4}$$

In Equation (4), $\mathbf{J_q}$ is the current density vector [A·m^{-2}]. It may be expressed with Ohm's law 5 where σ_q is the electric conductivity [S·m^{-1}] and ϕ the electric potential [V]. It should be noted that magnetic field had been neglected due to the low current level of 10 A.

$$\mathbf{J_q} = \sigma_q \boldsymbol{\nabla}\phi \tag{5}$$

DOI: 10.13009/EUCASS2023-419

Finally, ω_{Joule} can be expressed in function of J_q and σ_q as in relation 6.

$$\omega_{Joule} = \frac{\mathbf{J_q} \cdot \mathbf{J_q}}{\sigma_q} \tag{6}$$

The spatial extension of DC arcs convected by high-speed flows is limited by the sudden ignition of new plasma channels shortcutting the arc, known as the restrike phenomena in the literature. However, arc restrikes involve the very fast propagation of out-of-equilibrium and non-neutral plasma discharges such as streamers. Such models require timesteps and spatial discretisations far more restrictive than conventional CFD calculations. To tackle this problem, a macroscopic streamer model for restrike developed by A. Bourlet [10] has been implemented in TARANIS and used in this work. This approximate model that induces a negligible extra numerical cost to the CDF calculation has been validated on the LAERTE experimental facility at ONERA [11].
Briefly, the code finds the location of the maximum reduced electric field. In case of it exceeds the electrical breakdown field, the algorithm computes the electric field line from this maximum to either an electrode or a conductive cell in the arc plasma. Then a conductivity profile is applied around the computed field line to mimic the channel of a streamer discharge. If the heating of the streamer channel is high enough, its resistance may drop dramatically, leading to a n arc shortcut, which corresponds to a restrike event. This streamer is then convected and heated as a fraction of the total current flow.

2.3 Coupling scheme

The CWIPI library performs the coupling between CEDRE and TARANIS (Coupling With Interpolation Parallel Interface) [12]. At the end of each CEDRE iteration, the pressure, temperature, and velocity fields are sent through CWIPI to TARANIS. Then, TARANIS solves the current conservation equation. At the end of the TARANIS iteration, it sends back to CEDRE through CWIPI the Joule heating rate as depicted on Figure 1. This work does not consider magnetic forces and chemical source terms due to the low current level and the LTE approximation, respectively.

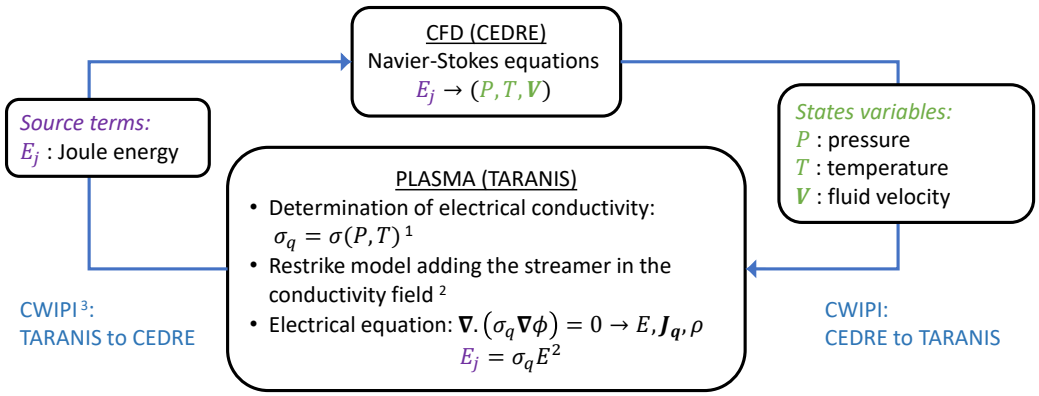

Figure 1: CWIPI coupling scheme, adapted from [13]

3. Simulation setup

The electrode responsibles for creating the electric arc used in this study is from S. Leonov [3] is located directly inside the fuel injector in the combustion chamber. Surrounding the injector is a ceramic material acting as an insulator, with the rest of the test facility earth grounded. This configuration is called PIM for Plasma Injection Module and described on Figure 2. The expected result is the ability of the electric arc to be positioned at the fuel-oxidant interface and add energy on the interface, the best place to enhance the chemical reaction.

3.1 SBR-50 facility

This study is adapted from experiment make on the supersonic part of the SBR-50 supersonic facility from Notre Dame University [4]. The dimensions are 610 mm long with an initial cross-section of 76x76 mm and an opening angle of 1° for the upper and lower walls [14]. The injector is placed at $x = 0.1$ m and $y = 0.0$ m, with a diameter of 3.2 mm (Figure 3). The flow of dry air in the duct has been heated using an Ohmic heater. In our simulation, thermodynamics

DOI: 10.13009/EUCASS2023-419

properties of dry air is obtained under the assumption of local thermodynamic equilibrium by using a tabulation of the A. D'Angola formulas [9].

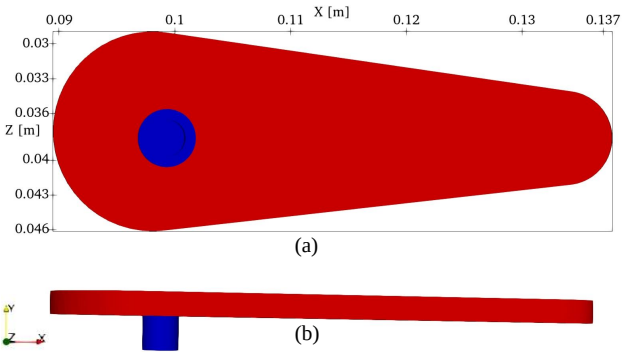

Figure 2: General scheme of a PIM. The anode is in blue and the insulated ceramic in red ; (a) top view ; (b) side view

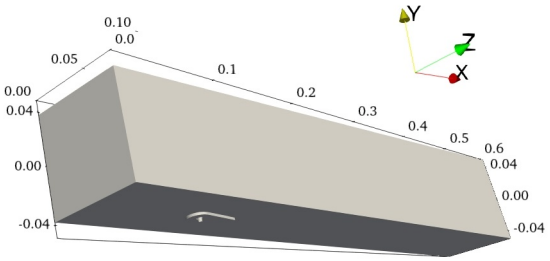

Figure 3: PIM position in the combustion chamber

3.2 Mesh and boundary conditions

Two meshes were used for this study. The first is optimised to study the restrike phenomenon in Section 6. It uses only tetrahedral cell ; the conditions of the fluid in the boundary layer is given by a law of the wall provided by CEDRE. It is enough to demonstrate the model's capacity to generate a restrike and describe the arc dynamic. The second one contains a boundary layer for a better evaluation of the interaction between arc root and bow shock in Section 4 & 5.

There is a general mesh used for CEDRE and TARANIS computation (Figure 4) with a refined zone in the vicinity of injector and ceramic (Figure 5) and a specific mesh for TARANIS to add the electrode body. The refining zone allows to reach characteristic sizes of the order of a 200 μm. It correspond with a zone from the connexion of the arc root with the cathode to continue in the flow along the PIM up to a sufficient distance. This distance allows the arc to develop in accordance with the experimental measurements made by S. Leonov. Typically twice the length of the insulated ceramic. In the rest of the combustor, the meshes have characteristic sizes of 3 mm to constrain the number of cells to 12.6 million for the CEDRE mesh without boundary and 16.8 million for the CEDRE mesh with the boundary layer and 0.6 million for the ceramic body.

A simulation is performed without arc discharge to obtain a quasi-static flow field. The flow is nonreactive, and the air properties are obtained from [9]. Inlet, injector and outlet boundary conditions are supersonic. The inlet-air is injected at P = 26 000 Pa, v = 940 m·s^{-1} and T = 297 K. While injector-air is injected at 170 000 Pa and a velocity of 400 m·s^{-1}. The wall condition is adiabatic for T and no-slip for u.
The ceramic body has been extruded for TARANIS mesh for an accurate computation of the electric field near the arc root. A I = 10 A current is imposed at the anode with a maximum voltage of 5 kV. A conductivity deposit of 10 S·m^{-1} is maintained during 10^{-6} s to initate the streamer. The anode boundary condition is extended to the entire injector and a 1 mm thick contour to avoid spike effects, which lead to a local temperature increase and contribute to the instability of calculation in CHARME.

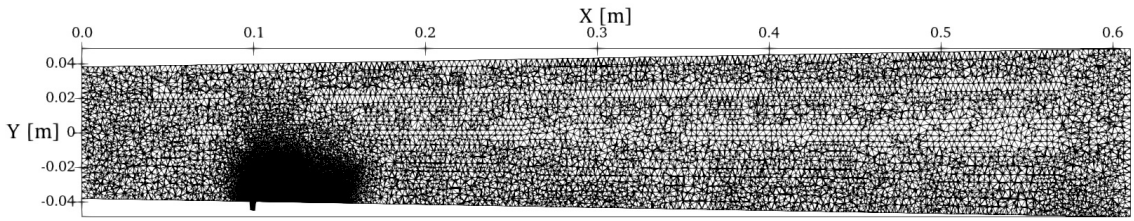

Figure 4: General mesh for CEDRE and TARANIS

DOI: 10.13009/EUCASS2023-419

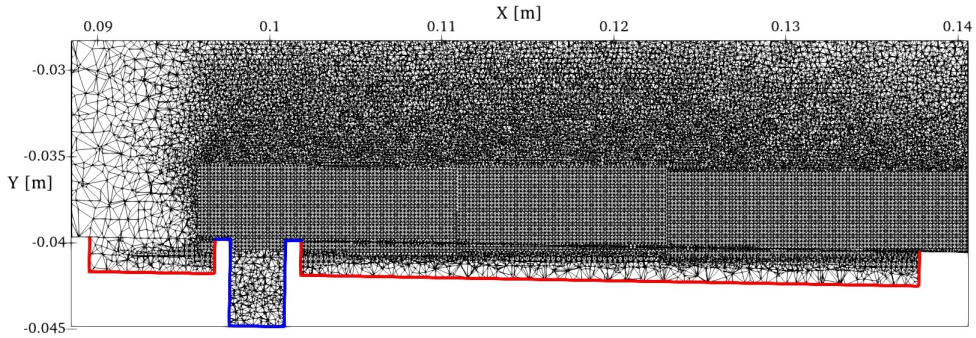

Figure 5: Refining mesh and ceramic body for TARANIS with electric boundary condition in: red for ceramic and blue for anode

4. Arc morphology

Several visualisations obtained with high-speed cameras [5, 14] provide information about arc morphology. These articles describe a vortical arc structure coupled with flow turbulences, namely a rapid growth between barrel shock and Mach disk, then a stabilisation in the turbulent jet. The arc length can be twice the ceramic's, and the diameter of vortical structures can be as large as the ceramic's. The width of the plasma depends on the temperature observed, but a diameter with a rough size of $1 - 3$ mm is observed.

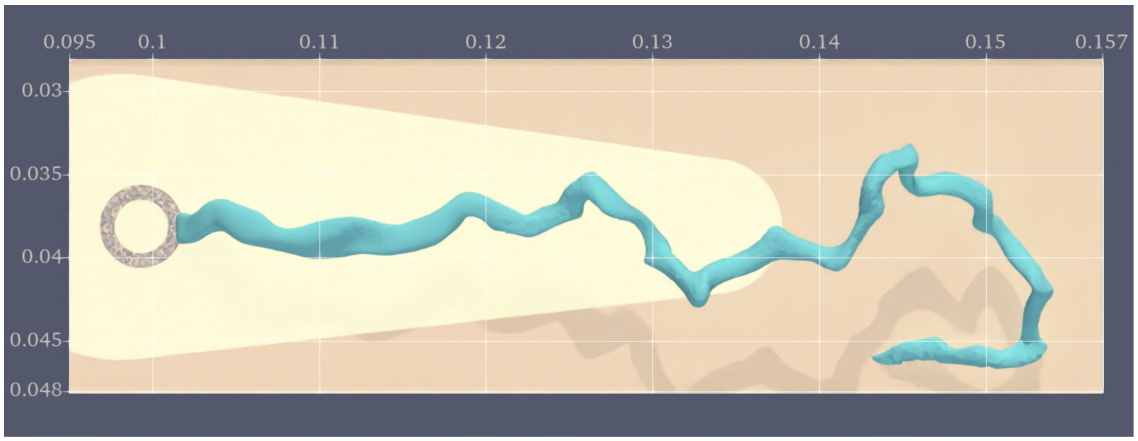

(a) A top view (X-Z plan)

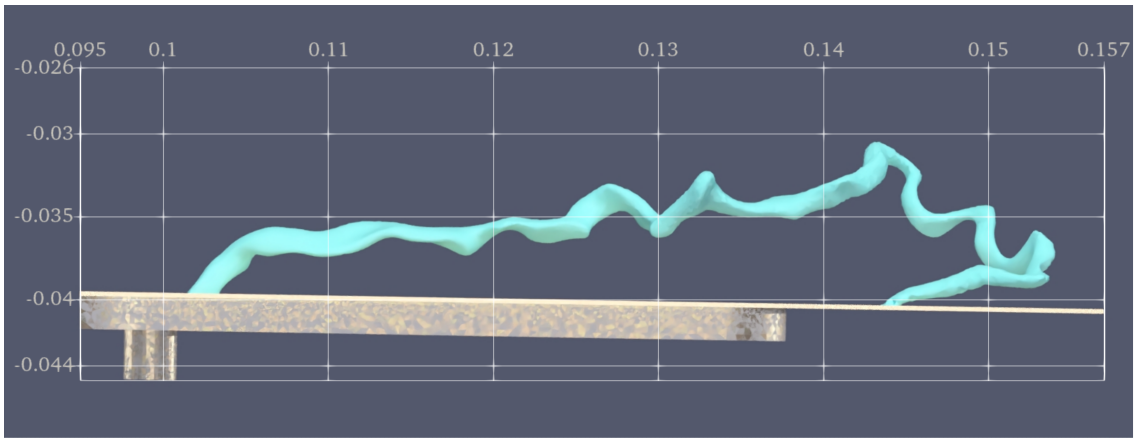

(b) An upstream direction view (X-Y plan)

Figure 6: Structure of the arc visualized with contour plot for $T = 8\ 000$ K and 68 μs after plasma ignition. All quantities are meters

DOI: 10.13009/EUCASS2023-419

(c) A front view (Y-Z plan)

(d) A downstream three-quarter view

Figure 6: Structure of the arc visualized with contour plot for $T = 8\ 000$ K and 68 μs after plasma ignition. All quantities are meters

The Figure 6 shows several numerical views of the arc once convected and sufficiently developed in the stream. Figure 6a shows that three-quarters of the arc parallels the flow. Only the downstream root is not aligned with the flow since the variations are between +4 and −4 mm on either side of the injector. That is because the first arc initiation took place on this side. Figure 6b shows the position of the arc in relation to the wall. It is not stuck to the bottom, caught in the boundary layer, but it is between 2 mm and 6 mm in the mixing layer. It also shows how the structures become more complex as they move further away from the injector. Figure 6c shows that the arc remains very localised compared with the injector size. Figure 6d gives a clearer picture of the 3D structure as a whole. That eases the visualisation of large structures in the downstream region and smaller ones in the middle of the arc. According to the experiment, the two codes allow a numerical qualitative reproduction of arc structure.

5. Arc-fluid interaction

5.1 Flow modification

One of the PIM's advantages is to optimise the catalyst effect by positioning the arc at the interface of oxidant-fuel in the mixing layer.

From the numerical Schlieren comparison between a flow with and without plasma in Figure 7, it can be seen that once developed and convected by the flow, the electric arc is positioned in the expected place, i.e. in the mixed layer after the barrel impact. That also shows the plasma-induced mixing effect in the recirculation zone and the appearance of a shock (in white on the Figure 7 right part) due to the positioning of the root of the arc close to the injector. The injected air plume is less blown with the plasma, which plays the part of a solid in the stream so that the injected air penetrates the stream better.

The Kelvin-Helmoltz-like instabilities observed in supersonic flow by [15] or Richtmeyer-Meshkov instabilities noticed by [16] and studied by [17] are pushed downstream and strengthen the mixing layer. The arc changes the barrel shock upstream too. Its root is more prominent, and considering the nonstationarity of the flow, that can affect the beat frequency of this shock and the downstream structures. In this case a *bubble* is produced every $\approx 10\ \mu$s.

One more way to convince of the improvement of mixing by adding the electrical arc is to compare on Figure 8 the difference between the mixing layer without and with the arc. In this goal, we use the two air annotations: the airflow is named *AIR_V*, and the injected one is called *AIR_I*. That allows us to follow the mixing steps. The arc modifies the flow structure downstream of the injector. The upper residual pockets of high *AIR_I* concentration structures are much thin and tortuous. It means the contact surface between *AIR_V* and *AIR_I* is augmented, and so the combustion in this system should be more efficient in the case of a reactive flow.

DOI: 10.13009/EUCASS2023-419

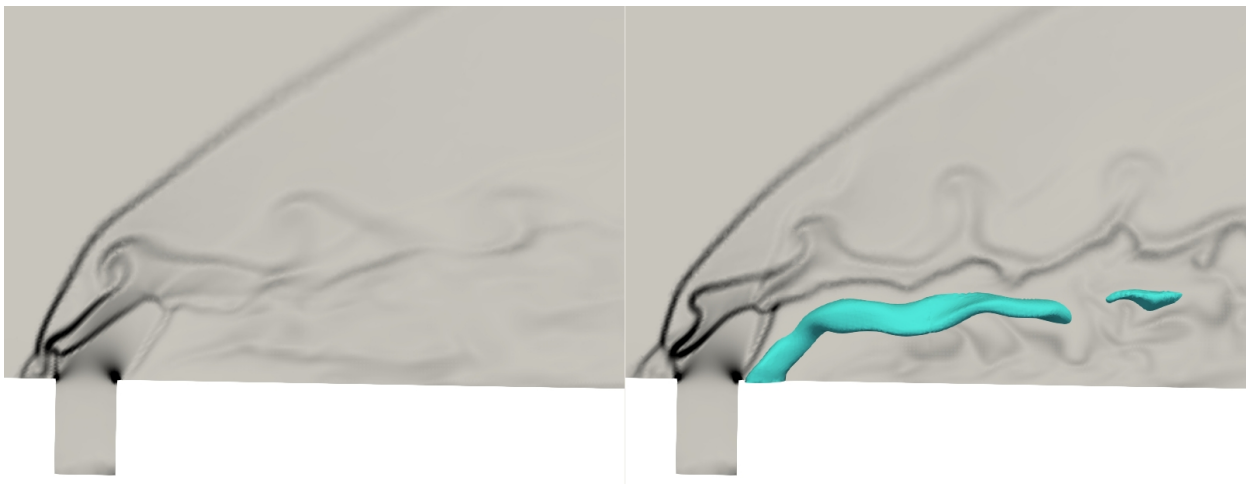

Figure 7: Numerical Schlieren $||\nabla\rho||$; left whithout Plasma - right with plasma in blue for $T = 8\,000$ K and 68 μs after plasma ignition

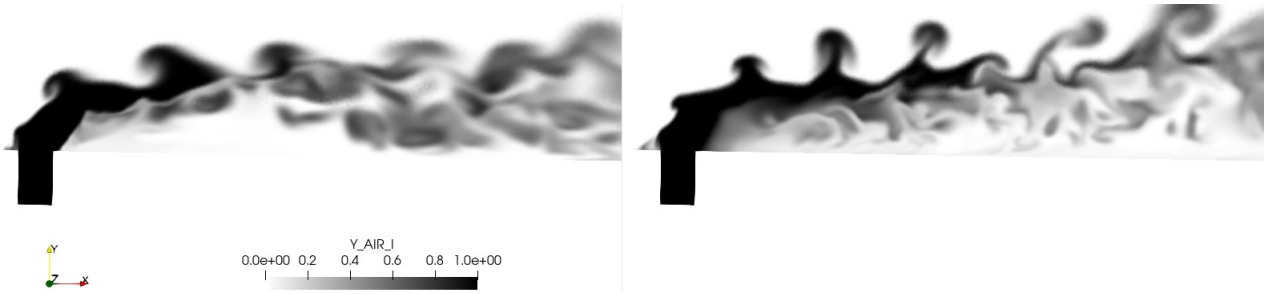

Figure 8: Mass fraction of AIR_I with (right) and without (left) plasma at the same time as Figure 7

5.2 Mixing effect

Figure 9 is used to illustrate the relative position of the mixing layer and plasma. For the three cross-sections perpendicular to the flow, the same four isolines in colour are drawn at $T = 3\,000$ K, 5 000 K, 7 000 K and 9 000 K to get an idea of the size of the electric arc and its positioning compared to the insulated ceramic. The mass fraction of the injected air is represented in grey cross-sections. A good mixing fraction can be defined as $30 - 70\%$ because two airs with the same properties are used for the simulation.
The first section of Figure 10 at $x = 0.102$ m shows that positioning the arc directly after the injector gives access to a mixing zone even though the diffusion of the injected species in the combustion chamber has not yet had time to take place. The high temperature of the arc help to accelerate the gas. Section (b), which corresponds to a horizontal part of the arc, is the most representative and also shows good arc positioning. The plasma's heat creates convection vortices that mix the two fluids with good efficiency from the positioning in the centre of the injected air. Finally, the last section (c) near the downstream root of the arc confirms this trend. The isolines on the bottom right are made by the root of the arc. The other part at 3 000 K shows the presence of a hot detached zone that goes on mixing. It can also be seen that the arc is mainly positioned between the most concentrated zones and those of medium mixing. The highly tortuous shape of the arc increases the contact surface, further improving mixing. To conclude from Figure 9, it may be seen that the arc's mixing function is not effective along its entire length but essentially from the upstream root to the downstream root. It is in this area that the mixing efficiency is relevant.

DOI: 10.13009/EUCASS2023-419

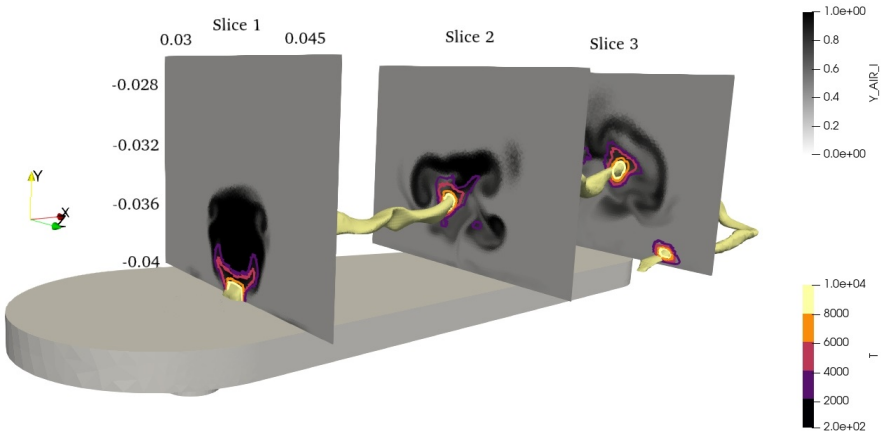

Figure 9: General view of clips on three key point : upstreamroot, horizontal section and downstreamroot of the arc

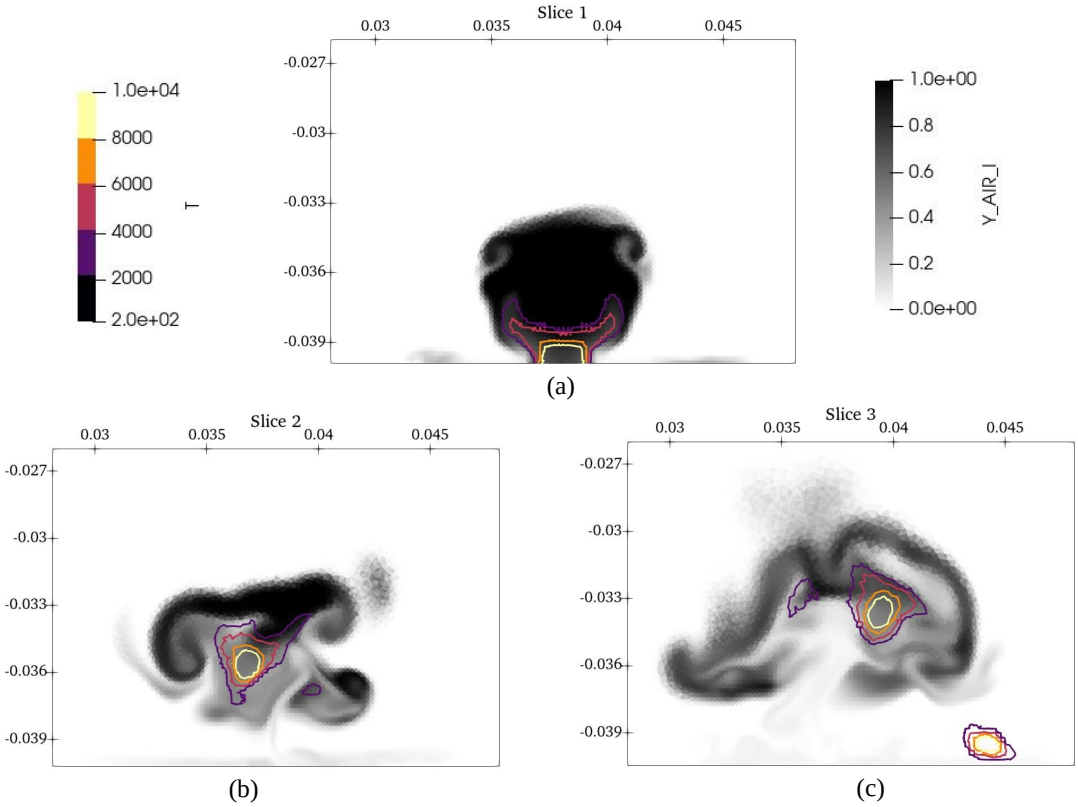

Figure 10: Clip at (a) x = 0.102 mm ; (b) x = 120 mm; (c) x = 136 mm showing position of arc in the mixing zone

To quantify this, it is possible to evaluate arc cells properties. The volume fraction of the arc is plotted depending on the fraction of injected air by cell in Figure 11. The criterion to determine if they belong is a temperature upper than 5 000 K. With this graph, it is possible to follow the action of the arc. For the Clip 1, orange curve, most of the arc's cells have a high fraction of injected air with a minimum of 0.6. The mixing effect or arc doesn't appear. For the Clip 2, purple curve, the mixing effect due to the heating is maximal with 35% of arc's cells which have between 40% and 60% of injected air. Some of them are always too much-injected air. For the Clip 3, violet curve, the peak between 40% and 60% is less high, but it is due to the arc's root in the boundary layer where no injected air comes. It explains the 35% of arc's cells with minus 10% of injected air.

DOI: 10.13009/EUCASS2023-419

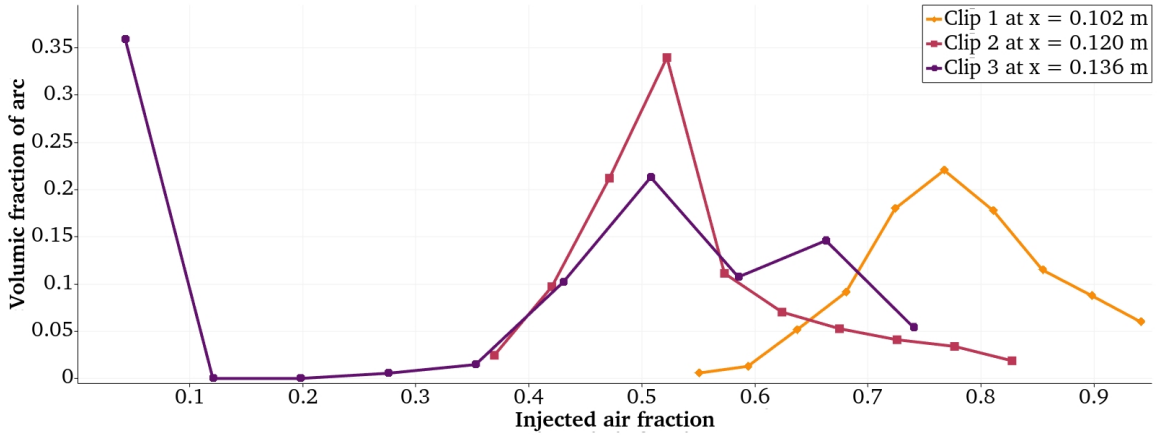

Figure 11: Mixing effect allong the arc. A medium injected air fraction show a good mixing. For exemple at x = 0.120 m, for 35% of the arc's cells the fuel injected fraction is 50%

6. Mechanism of restrike

The results obtained with the 13.2 million cells mesh are used for this part.
Another point of interest in this simulation is to follow the restrike mechanism. Figure 12 gives an idea of how the conductivity deposit is applied. The electric field line linked to the highest reduced electric field is not the shorter line from anode to cathode, as expected, even though there is no convection of heated cells. This initial conductivity deposit is not sufficiently heated to allow current to pass through.

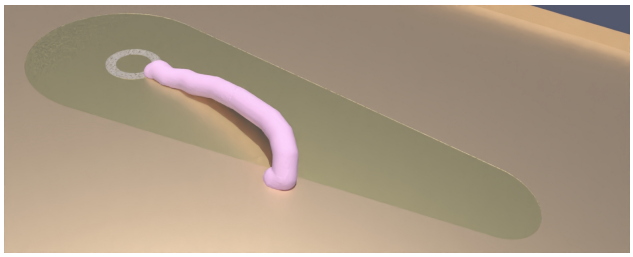

Figure 12: First connexion at $t = 0$ μs

When the cells reach a sufficient temperature, the current flows and the arc forms. It can be noticed on Figure 13. The pink part is the volume on which the model applies conductivity and is not hot enough to enable the current to go through ($T < 4000$ K). While the cyan part is a volume with high conductivity ($\sigma > 100$ S·m^{-1}) and high temperature ($T > 5\,000$ K) in which the electric current can go through. This volume results from other conductivity deposit, which was convected by the flow. The arc morphology is smoother than the other obtained in 4 due to the lower resolution of the boundary layer.
The picture at $t = 84$ μs shows a conductivity deposit between the arc and cathode since electric field lines are going by the arc. The length of the conductivity deposit is shorter than the first but competes with the arc. However, it is always in the same zone along the ceramic.
Between 85 μs and 89 μs, the flow convects the deposit, and some regions are heated, especially at the cathode surface and close to the arc where the velocity is lower. As long as the deposit time is 2 μs, there are more than three attempts on the same location to heat the flow. The heated cells are convected but do not have time to cool, and the conductivity deposition does sufficient warming. The setting up of the new arc begins with the extremities.
At $t = 91$ μs, the channel is heated enough, and now all the current passes through it. A new deposit is calculated, now between two parts of the arc. It shows the possibility of restrike not only between the arc and electrodes but also within the arc loops.
At $t = 95$ μs, the former part of the arc is cooled and convected while the new is also convected.

DOI: 10.13009/EUCASS2023-419

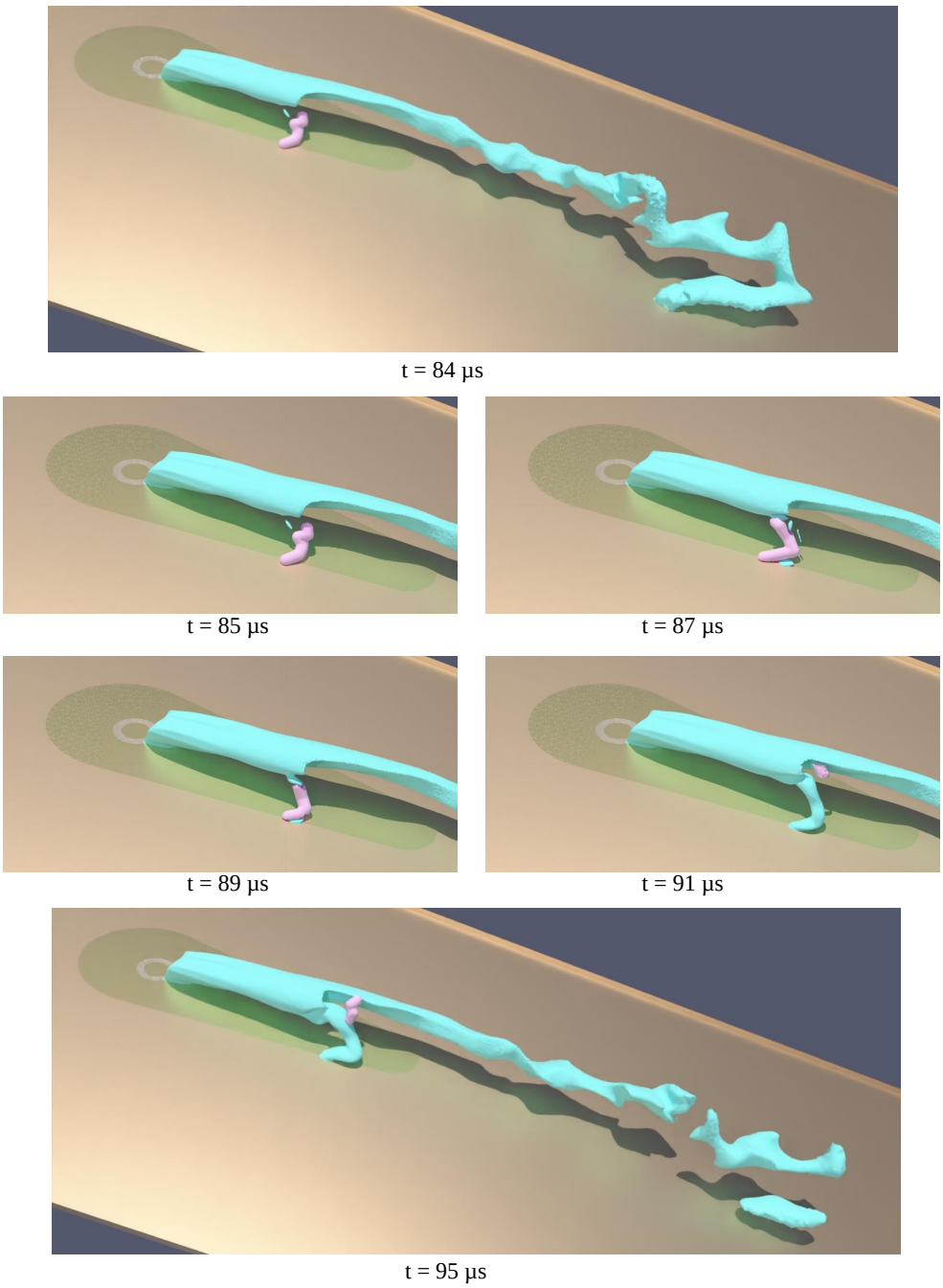

Figure 13: Mecanism of restrike; in blue the current electric arc and in purple the streamer

7. Conclusion

In this article, the plasma generated by the PIM has been modelled and simulated in the SBR-50 geometry with a flow at Mach 2.7 and a non-reactive crossflow. It was performed without initial energy deposition, that gives a more physical first restrike. The coupling between CEDRE and TARANIS enables to reproduce correctly the arc structure - lenght, size, tortuousity - observed experimentally and depending on the turbulence of the flow. The PIM is confirmed as a promising injection design by placing the arc in the injected stream; as well as enhancing the mixing through increase of the injector pulsation and size of the bow shock. It makes instabilities more thin and penetrating the flow. The mechanism of restrike was observed and detailed with a typical start place on the middle side of the PIM.

Parametric research will be performed on the importance of the lenght of the PIM on the blending. Especially the effect of the flow and electric voltage on the maximal length of the arc filament. A simulation with more than only one

DOI: 10.13009/EUCASS2023-419

restrike may show the influence from several restrikes movements on the flow. The next step is to simulate a simple set of reaction of H_2-O_2 oxidation to take in account the heat release from reaction and to observe the plasma's catalytic effect on the ignition time.

8. Acknowledgments

The authors would like to thank the French Defense Innovation Agency (AID), the French Procurement Agency (DGA) and the ONERA's scientific direction for funding and supporting the present work.

References

[1] A. A. Firsov, E. V. Dolgov, and S. B. Leonov, "Effect of DC-discharge geometry on ignition efficiency in supersonic flow," *J. Phys.: Conf. Ser.*, vol. 1112, p. 012011, Nov. 2018.

[2] S. B. Leonov and D. A. Yarantsev, "Plasma-induced ignition and plasma-assisted combustion in high-speed flow," *Plasma Sources Sci. Technol.*, vol. 16, pp. 132–138, Feb. 2007.

[3] S. B. Leonov, A. Houpt, and B. Hedlund, "Experimental Demonstration of Plasma-Based Flameholder in a Model Scramjet," in *21st AIAA International Space Planes and Hypersonics Technologies Conference*, (Xiamen, China), American Institute of Aeronautics and Astronautics, Mar. 2017.

[4] P. Andrews, P. Lax, S. Elliott, A. Firsov, and S. Leonov, "Flow Characterization at Heated Air Supersonic Facility SBR-50," *Fluids*, vol. 7, p. 168, May 2022.

[5] S. B. Leonov, B. E. Hedlund, and A. W. Houpt, "Morphology of a Q-DC Discharge within a Fuel Injection Jet in a Supersonic Cross-Flow," in *2018 AIAA Aerospace Sciences Meeting*, AIAA SciTech Forum, American Institute of Aeronautics and Astronautics, Jan. 2018.

[6] S. B. Leonov, Y. Isaenkov, D. Yarantsev, I. Kochetov, A. Napartovich, and M. Shneider, "Unstable Pulse Discharge in Mixing Layer of Gaseous Reactants," in *47th AIAA Aerospace Sciences Meeting including The New Horizons Forum and Aerospace Exposition*, (Orlando, Florida), American Institute of Aeronautics and Astronautics, Jan. 2009.

[7] G. Pelletier, M. Ferrier, A. Vincent-Randonnier, V. Sabelnikov, and A. Mura, "Wall Roughness Effects on Combustion Development in Confined Supersonic Flow," *J Propul Power*, vol. 37, pp. 151–166, Jan. 2021.

[8] A. Refloch, B. Courbet, A. Murrone, P. Villedieu, C. Laurent, P. Gilbank, J. Troyes, L. Tessé, G. Chaineray, J. B. Dargaud, E. Quémerais, and F. Vuillot, "CEDRE Software," *Aerospace Lab*, p. p. 1, Mar. 2011.

[9] A. D'Angola, G. Colonna, C. Gorse, and M. Capitelli, "Thermodynamic and transport propertiesin equilibrium air plasmas in a wide pressure and temperature range," *Eur. Phys. J. D*, vol. 46, pp. 129–150, Jan. 2008.

[10] A. Bourlet, J. Labaune, F. Tholin, A. Vincent, F. Pechereau, and C. O. Laux, "Numerical model of restrikes in DC gliding arc discharges," in *AIAA SCITECH 2022 Forum*, (San Diego, CA & Virtual), AIAA, Jan. 2022.

[11] A. Bourlet, J. Labaune, F. Tholin, A. Vincent-Randonnier, F. Pechereau, and C. O. Laux, "Restrike model for an MHD solver: application to plasma assisted supersonic combustion in scramjet," p. 10 pages, 2022.

[12] E. Quémerais, "Coupling with interpolation parallel interface," 2016.

[13] S. Rassou, D. Packan, P.-Q. Elias, F. Tholin, L. Chemartin, and J. Labaune, "Numerical modeling of a glow discharge through a supersonic bow shock in air," *Physics of Plasmas*, vol. 24, p. 033509, Mar. 2017.

[14] S. Elliott, P. Lax, S. B. Leonov, C. Carter, and T. Ombrello, "Acetone PLIF visualization of the fuel distribution at plasma-enhanced supersonic combustion," *Exp Therm and Fluid Sci*, vol. 136, p. 110668, Aug. 2022.

[15] W. C. Wan, G. Malamud, A. Shimony, C. A. Di Stefano, M. R. Trantham, S. R. Klein, D. Shvarts, C. C. Kuranz, and R. P. Drake, "Observation of Single Mode, Kelvin Helmholtz Instability in a Supersonic Flow," *Phys. Rev. Lett.*, vol. 115, p. 145001, Oct. 2015.

[16] S. B. Leonov, "Electrically Driven Supersonic Combustion," *Energies*, vol. 11, p. 1733, July 2018.

[17] O. A. Azarova, "Generation of richtmyer-meshkov and secondary instabilities during the interaction of an energy release with a cylinder shock layer," *Aerospace Science and Technology*, vol. 42, pp. 376–383, Apr. 2015.